World Electric Vehicle Journal

MDPI

Article

Design and Construction of a Multipole Electric Motor Using an Axial Flux Configuration

Adrián González-Parada [1,2,*], Francisco Moreno Del Valle [1] and Ricard Bosch-Tous [1]

[1] Department of Electrical Engineering, ETSEIB, Polytechnic University of Catalonia, 08028 Barcelona, Spain; francisco.moreno.del@upc.edu (F.M.D.V.); ricard.bosch@upc.edu (R.B.-T.)
[2] Department of Electrical Engineering, DICIS, University of Guanajuato, Salamanca Guanajuto 36787, Mexico
* Correspondence: adrian.gonzalez-parada@upc.edu or gonzaleza@ugto.mx

Abstract: In the transportation industry, the use of renewable energies has been implemented in conjunction with the development of higher-power electric motors and, consequently, the development of intelligent control systems for torque and speed control. Currently, the coupling between both systems is being developed through mechanical systems, affecting the efficient transmission of energy and the useful life of the components. On the other hand, new configurations of electric motors are being developed, such as axial flux motors (AFM), because these can be coupled directly without a mechanical coupling, given their characteristics of high torque at low speeds. In the present work, an innovative design of a multipole axial flux motor (MAFM) is introduced. General criteria for the design and construction are presented considering the geometry in axial flux and permanent magnets. The performance of the system is evaluated through finite element magnetic simulations (FEMM) and compared with experimental measurements of the developed prototype; confirming the effectiveness of the design, obtaining torques of up to 1.784 Nm without extra mechanical couplings and maximum speed regulation errors of 8.43%. The motor was controlled by a digital pole switching system whit six control mode, applied to a permanent magnet MFA for speed and torque control at constant speed. This control can be extended to conventional radial flux electric motor configurations and intelligent traction applications, based on torque demand.

Keywords: multipole motors; permanent magnet; axial flux; U coil

Citation: González-Parada, A.; Moreno Del Valle, F.; Bosch-Tous, R. Design and Construction of a Multipole Electric Motor Using an Axial Flux Configuration. *World Electr. Veh. J.* **2024**, *15*, 256. https://doi.org/10.3390/wevj15060256

Academic Editors: Youguang Guo, Gang Lei and Xin Ba

Received: 12 April 2024
Revised: 28 May 2024
Accepted: 3 June 2024
Published: 12 June 2024

1. Introduction

The electric motor (EM) plays a predominant role in the industrial system, consuming up to 65% of the total electrical energy demand, which represents 38.4% of the total electrical energy consumed [1]. Furthermore, their reliability and efficiency characteristics have driven their use in the green transportation industry as backup traction sources [2] and even as primary traction sources as in the case of [3]. The entry of EM in the automotive industry in conjunction with the accessibility and advancement in power electronics controlled by digital systems has led to the development of motors with emerging technologies such as permanent magnet motors (PMM), switchable reluctance motors (RM) and synchronous reluctance motors that exceed 95% efficiency. Despite the great development in areas of EM design and operation, these, like internal combustion engines, continue to depend on mechanical systems such as gear trains (transmission system) to convert their high speed with low torque to low speeds with high torque, resulting in more expensive, heavy, inefficient applications that are more susceptible to failure than they should be. They would allow energy consumption to be limited to the minimum necessary, increasing its autonomy and efficiency.

The development of electric motors in automotive vehicles and the advancement of power electronics have led to emerging technologies such as the development of permanent magnet motors, commutable reluctance motors (CRMs), and synchronous reluctance

motors (SRMs), which exceed 95% efficiency [1–3]. However, these motors continue to rely on mechanical systems like gear trains to convert their high speed with low torque to low speed with high torque, resulting in expensive, heavy, inefficient, and failure-prone applications. Exploration of other motor configurations, such as axial flux motors, has proven to be ideal for low speed, and high torque applications [4]. These motors dispense with mechanical couplings and are complemented by a digital speed and torque control system, which allows energy consumption to be limited to the minimum necessary, increasing the autonomy and efficiency of the vehicle.

This article describes the general aspects of the design, construction, validation and testing of a multipolar electric motor in axial flow configuration. In Section 2.1, the theoretical aspects of the design of a multi-pole electric machine in axial flow configuration are mentioned, based on the power delivered, efficiency and duty cycle of the machine. For the design, the availability of commercial components was considered, such as magnets for the rotor and ferromagnetic cores for the design of the stator poles, and in Section 2.2, the design of the U coil for the stator design, is shown. Based on these and applying the general equations, the evaluated design was obtained.

Section 2.3 shows the design of the rotor, considering the geometry of the proposed magnets according to the commercial dimensions. In Section 2.4, the finite element simulation is carried out with the objective of obtaining the theoretical results and, from these, comparing them with the experimental results from the construction of the prototype.

Section 2.5 mentions the type of control developed for this multipolar electric machine, where from each of the polar sections of the stator, the connection and disconnection arrangement are made to vary the number of poles without losing the delivered torque. A more complete description of the motor control is shown in [5].

Section 3 gives the construction parameters and equipment used in the evaluation of the developed engine, and a comparison is made of the results obtained both in the simulation and in the laboratory tests.

2. Materials and Methods

2.1. Axial Flux Motor Design

The dimensional design of electric motors depends on the application of interest, the supply voltage V and the current I_r, which will be reflected in the power delivered P_d by the motor. The power of the motor is a function of its efficiency K_e and duty cycle K_d.

$$P_d = m \cdot K_e \cdot K_d \cdot V \cdot I_r \tag{1}$$

where, K_d depends on the number of rotor poles P_r and the number of stator poles P_s, considering the angle between stator poles θ.

$$K_d = \frac{\theta P_r}{360} \cdot \frac{P_s}{2} \tag{2}$$

In [6,7], the expression has been developed for V as a function of the dimensions of the stator, according to Figure 1:

$$V = (1 - 1/\propto)\omega_m B T_{ph} \cdot \left(\frac{D_2 + D_1}{4}\right) \cdot \left(\frac{D_2 - D_1}{2}\right) \tag{3}$$

where

$\propto$ is the ratio of inductances when the pole is aligned L_a with the rotor and when the pole is unaligned L_u.

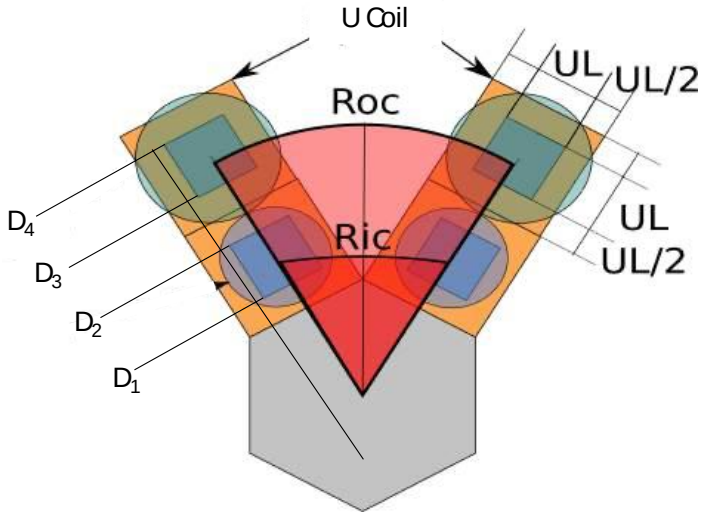

Figure 1. Geometric arrangement of coils and adjacent permanent magnets.

$$\propto = L_a / L_u \tag{4}$$

B = average flux density.
T_{ph} = # of turns per phase.
ω_m = rotor speed.

The magnetic charge is expressed as a function of the dimensions of the stator, T_{ph}, I_r, and the number of phases (m):

$$A_{sp} = m \cdot \frac{2 T_{ph} I_r}{\pi D_{av}} \tag{5}$$

where

$$D_{av} = \frac{D_1 + D_2 + D_3 + D_4}{4} \tag{6}$$

Considering that the power duty cycle factor is constant [4], the power delivered by the motor based on the dimensions of the stator will be

$$P_d = K_{pd} \cdot \frac{D_2 + D_1}{2} \cdot \frac{D_2 - D_1}{2} \cdot \frac{D_1 + D_2 + D_3 + D_4}{4} \tag{7}$$

where

$$K_{pd} = 4 K K_e K_d K_u B A_{sp} \omega_m \tag{8}$$

K = 0.1964, K_e is the efficiency, K_d is the duty cycle, and $K_u = 1 - 1/\alpha$.

According to Figure 1, the average working diameters can be obtained as

$$R_{ic} = \frac{D_1 + D_2}{2} \tag{9}$$

$$R_{oc} = \frac{D_3 + D_4}{2} \tag{10}$$

The minimum thickness for the poles in the stator can be determined as

$$L_i = \frac{D_2 - D_1}{2} \tag{11}$$

The working power can be determined as

$$P_d = K_{pd} L_i R_{oc} R_{ic} \tag{12}$$

R_{oc} and R_{ic} are restricted to parameters that can be the diameter of the shaft, dimensions of the pole winding, etc.

The AFMs are ideal for applications where the space determined for each element must be reduced to a minimum [8,9]. In the case of axial flux motor and generator design, the component that determines the final dimensions of the motor is the stator (Figure 1) since it provides an effective working area and the minimum diameter of the rotor [9,10].

In AFMs, the design of the stator depends only on the number and dimensions of the coils. The stator is made up of U-type coil (UC) and modular coils, and its topology consists of two-series windings arranged on each leg of the UC [11,12]. A bar is placed on top of the UC that simulates the part of the rotor that interacts magnetically with the magnetic flux field generated by the UC windings. Figure 2 shows the UC topology.

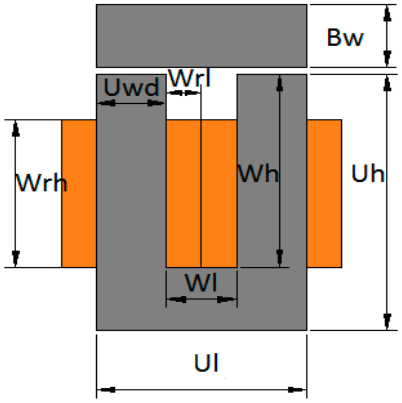

Figure 2. General scheme of UC.

where
Bw = bar width (rotor);
Ul = length;
Uh = height;
Uwd = leg width;
Wl = window width;
Wh = window height;
Wrl = copper winding height;
Wrh = copper winding width.

2.2. U-Type Coil (UC) Design

The magnetic circuit shown in Figure 3 is derived from the scheme presented in Figure 2.

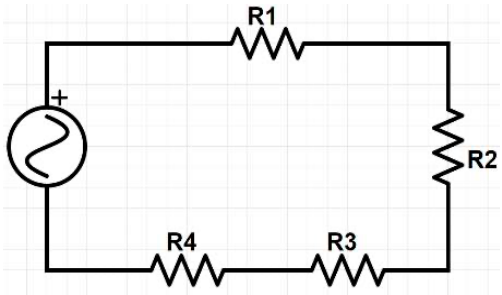

Figure 3. Model of the magnetic bar circuit (rotor), between iron and windings.

In the magnetic circuit of Figure 3, the series-connected windings are modeled as a single source of magnetomotive force (MMF) in Ampere-turns. *R*1 and *R*3 represent the average reluctance of the gap between the UC and the top bar (rotor), *R*2 is the average

reluctance of the top bar, and $R4$ represents the average UC reluctance in A/Wb. The average reluctance (R) is defined by Equation (13).

$$\mathcal{R} = \frac{MPL}{\mu_m A_c} \tag{13}$$

where

MPL = mean magnetic path length;
μ_m = magnetic permeability of the medium Wb/m^{2}A;
A_c = cross-sectional area m^2.

The maximum magnetic field in the UC will be in accordance with Equation (14).

$$B_{NTU} = \frac{8.84 i W_h (W_h - D)(\mathcal{R}_1 + \mathcal{R}_2 + \mathcal{R}_3 + \mathcal{R}_4)}{D^3 \pi \left(A_c + \sqrt{A_c} l_G \ln \frac{2W_h}{l_G} \right)} \tag{14}$$

where

l_G = gap length;
R_n = reluctance of each component of the magnetic circuit ($R_1 \ldots \ldots R_4$).

The magnetic field density in the UC depends on the material that is used, the geometric configuration, and the spacing between the UC and the upper bar (rotor) [13].

2.3. Rotor Design

The rotor is made up of two circumferences that inscribe the polygon formed by the number of magnets to be used (Nm), with an internal (R_{ic}) and external (R_{oc}) radius, respectively, which have the permanent magnets (IPs) distributed uniformly on their perimeters. Both circumferences mainly depend on the dimensions of the stator, according to Figure 4.

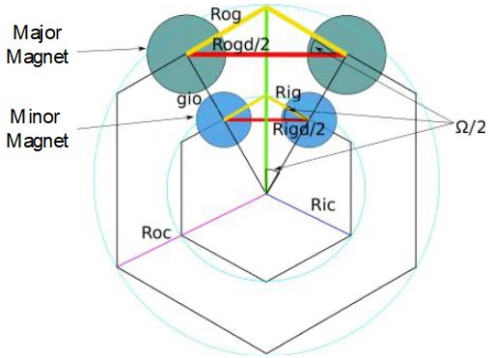

Figure 4. Arrangement of permanent magnets of rotor on inscribed polygon.

The minimum radius of the rotor depends on the number of IPs, the radius of the internal IPs (R_i), the radius of the external IPs (R_o), and UL, which is the length of the leg of the U-type core (UTC). Figure 4 shows the diagram used to obtain the internal IP radius according to Equation (15) [14].

$$R_{ig} = R_i + g_{mi} \tag{15}$$

where R_{ig} = internal IP radius (R_i), and g_{mi} = separation distance between internal IPs.

For the construction of a rotor with commercial components, it is necessary to meet the following conditions:

$$R_0 < 2U_L - R_i \tag{16}$$

$$0 < gio < 2U_L - R\_R_0 i \tag{17}$$

2.4. Behavior Simulation

In permanent magnet axial flux motors (PMFAMs), the only source of losses in the ME is mainly generated in the stator (core losses, copper losses, dispersion flux losses, etc.). The magnitude and weighting of these depend on the materials, the winding, and the design of the stator. Therefore, it is necessary to use tools that allow for the exploration of a wide range of possible configurations. Finite Element Analysis Magnetic Software (FEMM 4.2) is the tool currently used to evaluate the design and performance of an EM.

Analysis of conventional radial flux motors using the finite element method (FEM) is carried out by analyzing a two-dimensional cross-section of the motor, but for axial flux motors (AFMs), this is not possible due to magnetic fields are in the radial direction and parallel to the simulation plane. To overcome this limitation, the AFM is visualized as a bipolar linear motor, rearranging the circularly arranged poles in the AFM to a new linear arrangement, as shown in Figure 5a,b.

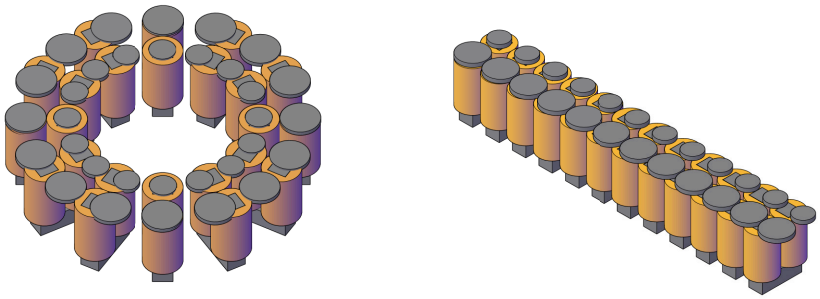

(a) Circular Distribution (b) Linear Distribution

Figure 5. Three-dimensional model for analysis using finite element analysis (FEA).

In the linear rearrangement of the magnetic poles of the AFM, the minor and major magnets are not aligned (rotor magnetic poles) to the poles of the U-type coils (rotor magnetic poles) because the major magnets and minor magnets are arranged on perimeters of different lengths. For this reason, the analysis must be divided into two analyses: a two-dimensional cross-sectional analysis for the interaction of the U-type coil poles with the larger magnets (Figure 6a) and a second two-dimensional cross-sectional analysis for the interaction of the U-type coil poles with the smaller magnets (Figure 6b).

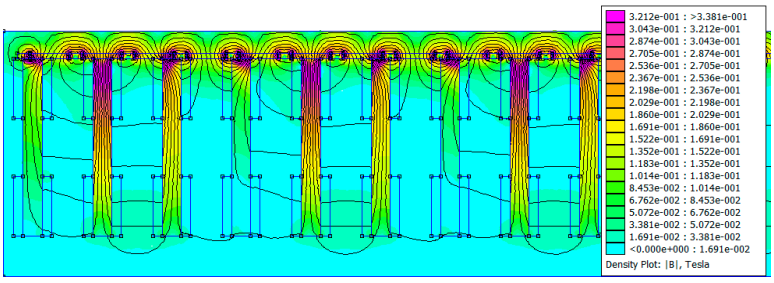

(a) UC and Major magnet simulation

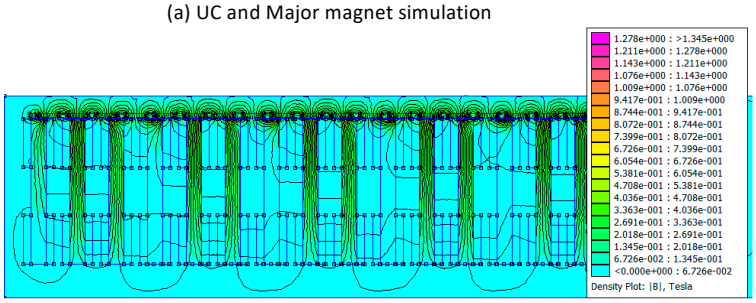

(b) UC and Minor magnet simulation

Figure 6. Simulation of FEA of redistributed AFM in linear motor.

A simulation was carried out by modifying the characteristics and positions of the electrical circuits of the stator coils and the permanent magnets of the rotor. Figure 6 shows the magnetic flux density for the displacement of the rotor to the left in relation to the coils. The previous procedure was carried out iteratively on the cross-sections of Figure 6 to simulate a complete revolution (forty-eight sequences) at different supply currents for each of the six torque settings.

From the simulations developed in FEA and the AFM evaluation, the speed curves in relation to the torque were obtained for each of the six proposed torque configurations.

2.5. Motor Control

Rotation in permanent magnet motors (PMMs) is produced by the interaction of an alternating magnetic field with a static magnetic field, generating attractive or repelling forces depending on the present magnetic polarity. To calculate the rotational speed in RPM for a PMM, one must consider the time the stator magnetic poles remain active in each magnetic polarization sequence and the time it takes to switch from one sequence to another [15–17].

Considering that the switching time between sequences is negligible and that the stator magnetic poles are active for T_s seconds per sequence, then the rotational speed in RPM for a PMM of order n can be calculated using Equation (18).

$$S_{RPM} = \frac{1}{SPRT}\frac{1}{T_s}\frac{60\ \text{seg}}{\text{min}} = \frac{5}{(2^{n-2})T_s} = \frac{5f_s}{2^{n-2}} \tag{18}$$

where

f_s = commutation frequency per second;

SPR = sequences per rotor revolution.

The rotational speed in terms of the electrical power frequency can be determined by

$$S_{RPM} = \frac{30f_E}{2^{n-2}} = \frac{30}{(2^{n-2})T_E} \tag{19}$$

where

f_E = electrical frequency $(1/6T_S)$;

T_E = full cycle period.

Equation (19) is also applicable to the case of a sinusoidal three-phase supply. Figure 5 shows the speed variation with respect to electrical frequency (f_E) for different values of order n (Figure 7).

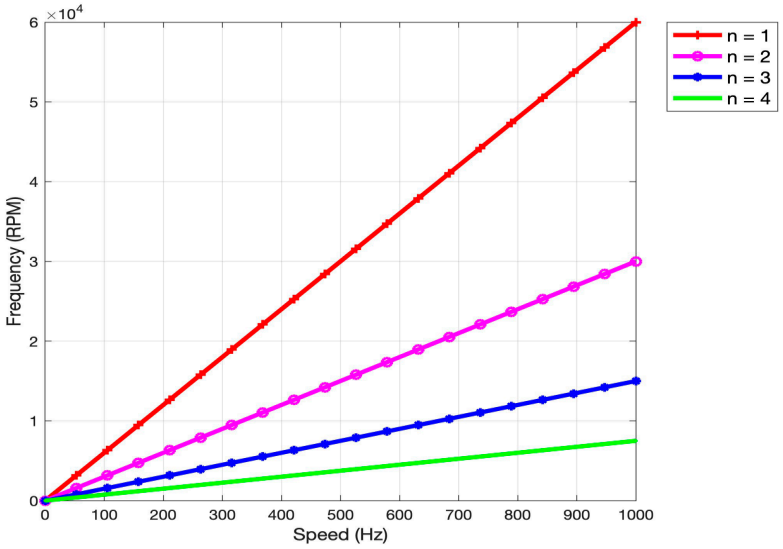

Figure 7. Speed vs. electrical frequency for different values of n.

In a first-order configuration (n = 1), at least three coils are needed for three phases, while in larger configurations (n = 2, n = 3, n = n, etc.), it is possible to use a single coil per phase, although this will reduce the delivered torque. The fourth-order configuration (n = 4) with twelve poles in the stator ($3n$ = 12) and sixteen in the rotor (2^n = 16) allows for the evaluation of different partial applications of torque. The AFM allows the applied torque to be modified according to the number of active stator poles, and it can have up to six torque configurations depending on the commutation of the stator coils.

In the design of the motor, six connection configurations are used for speed and torque control. These consist of changing the connection of the number of stator poles that are interacting with the rotor poles; considering that the use of the stator coils is limited to the minimum in configuration number 1 (one coil per phase), and in configuration 6, the operation is carried out at the maximum mechanical power available, since all the coils (four coils) are used per phase [17–19]. The development of the control system is shown more extensive in [5], where the six different control configurations and their behavior are analyzed.

Figure 8 shows the commutation of the twelve coils in the stator, with three different states: positive activation (rising), negative activation (descending), and no activation (flat).

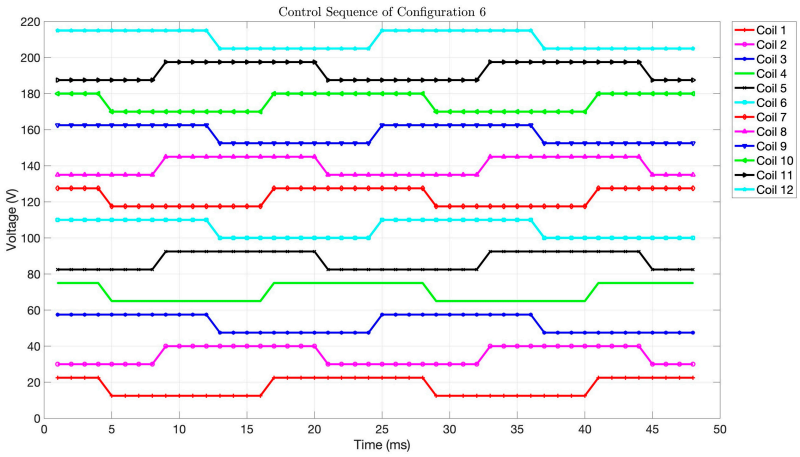

Figure 8. Commutation signals of the twelve magnetic poles (configuration 6). Reprinted from Ref. [5].

The sequential control method for changing the rotational speed of the AFM modifies the electrical switching frequency of the stator coils to achieve a digital switching frequency in a digital system. Equation (20), which expresses speed as a function of electrical switching frequency, is obtained by combining Equations (18) and (19) in terms of T_s.

$$S_{RPM} = \frac{7.5}{6T_s} = \frac{5}{4T_s} \tag{20}$$

The system allows for changing the three-phase frequency to vary the speed and the independent commutation of the coils to modify the torque.

3. Results

3.1. Motor Design and Construction

An AFM with 12 ($3n$ with n = 4) poles in the stator and 16 ($2n$) poles in the rotor was constructed according to the dimensions shown in Figure 9.

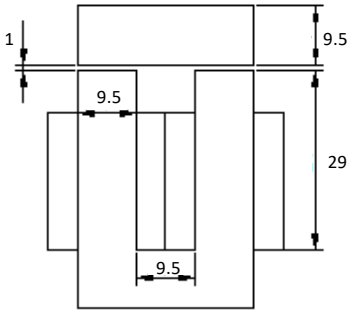

Figure 9. UTC dimensions in mm (Core EI-750).

Once the geometry of the AFM is defined, the magnetic interaction between the stator and rotor magnetic dipoles can be evaluated to determine if it is effective in generating motion in the motor. This magnetic interaction depends on the magnetic fields between the adjacent stator (EMD) and rotor (RMD) magnetic dipoles having the same shape and magnitude. Equation (21) provides the intensity of the magnetic field H for the type of IP used.

$$H = \frac{B_r}{2}\left(\frac{l + L_m}{\sqrt{(l + L_m)^2 + \frac{D^2}{4}}} - \frac{l}{\sqrt{l^2 + \frac{D^2}{4}}}\right) \quad (21)$$

where

B_r = remanent magnetic field density of the material;
l = distance from the center of the magnet to the point of measurement;
L_m = magnet thickness;
D = magnet diameter.
The main AFM parameters are shown in Table 1.

Table 1. Input and output parameters for the AFM.

Dimensional Design with 12/16 Poles in Stator/Rotor				
Parameters	**Variable**	**Definition**	**Value**	**Unit**
Input	U_l	U core length	9.5	mm
	N_C	Stator pole number	12	Parts
	N_m	Rotor pole number	16	Parts
	N_L	Lamination number	23	mm
	E_L	Lamination width	0.5	mm
	g_{mmd}	Minimum perimeter separation between major and minor magnets	4	mm
	g_{mimod}	Minimum separation desired between major magnet and minor magnet	6	mm
Output	r	Radius of inscribed polygon of stator coils	44.5	mm
	R_{ic}	Radius of inscribed polygon of minor magnets	44.8	mm
	R_{oc}	Radius of inscribed polygon of major magnets	64.1	mm
	g_{min}	Minimum perimeter separation between minor magnets	4.4	mm
	g_{mom}	Minimum perimeter separation between major magnets	5.5	mm
	g_{mimod}	Minimum separation desired between major magnet and minor magnet	3.1	mm
	D_i/R_i	Minor magnet diameter	12.7	mm
	D_o/R_o	Major magnet diameter	19.0	mm

If the distance between the stator and the rotor is small (0.2 mm), the interaction between the DPM and the U-type coil (UC) is produced by the incidence of the normal component of the magnetic field to the plane of the simulation. The curve of Figure 10 shows the effective magnitude of B of the UC is equal to or above trajectory B, confirming that the most effective interaction occurs in the central part of the design.

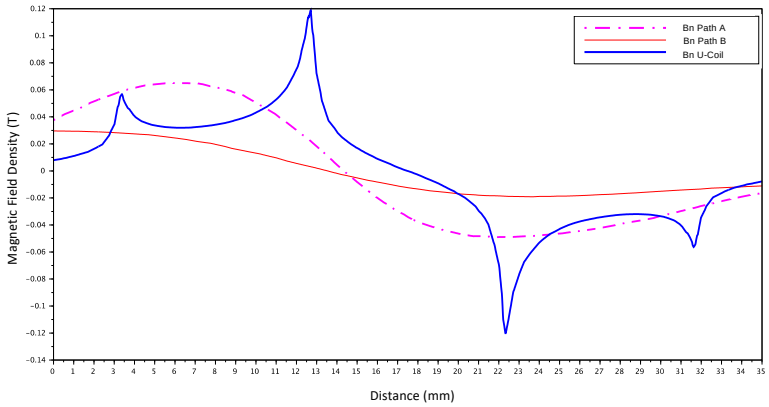

Figure 10. Magnitude of normal B generated by UC and by DPM.

The constructive values of the built prototype are presented in Table 2, which includes the overall dimensions of the device.

Table 2. Input and output parameters for the MAF design.

Input and Output Parameters				
Parameters	**Variable**	**Definition**	**Value**	**Unit**
Input	UL	Distance between U-type coils and bar (rotor)	9.5	mm
	Wh	Window height	29	mm
	Wl	Window length	9.5	mm
	Uwd	Window width	9.5	mm
	EL	Lamination thickness	0.5	mm
	Nl	Lamination number	23	Part
	μ_m	Air relative permeability	1	NA
	μ_{UTC}	Relative core permeability	4316	NA
	μ_b	Relative bar (rotor) permeability	1.04	NA
	B_d	Magnetic field density	4	Tesla
	AWG_{Cu}	Copper wire gauge	24	AWG
Output	i_{max}	Current	0.803	A
	R_c	Winding resistance	4.77	Ω
	L_c	Winding inductance	44.89	H
	V_{cd}	CD voltage	3.83	V
	N	Total	376	Part
	NL	Layer number	8	Part
	$NCpL$	Number of conductors per layer	47	Part
	AWG_l	Copper conductor total length	60.16	m
	AWG_w	Copper winding total weight	0.109	kg

3.2. Behavior Assessment

For the evaluation of the prototype, it is necessary to use a known system that can be programmed with different types of variable loads, with respect to speed and frequency, in such a way that they meet the necessary parameters for the characterization of the electric motor. For this evaluation, a variable load dynamometer was directly coupled to the motor shaft, which is governed by the control system and a data acquisition system, with which the necessary evaluations can be programmed to determine the main characteristics of the prototype.

The Lab-Volt measurement system shown in Figure 11 consists of the Lab-Volt 8960—a four-quadrant source/dynamometer module configured in dynamometer mode to measure speed, torque, and mechanical power delivered. Also included is the Lab-Volt Series 9063-02 Data Acquisition and Control Interface (DACI) and the free Lab-Volt Electromechanical Systems Control and Data Acquisition Software (LVDAC-EMS 9063-A).

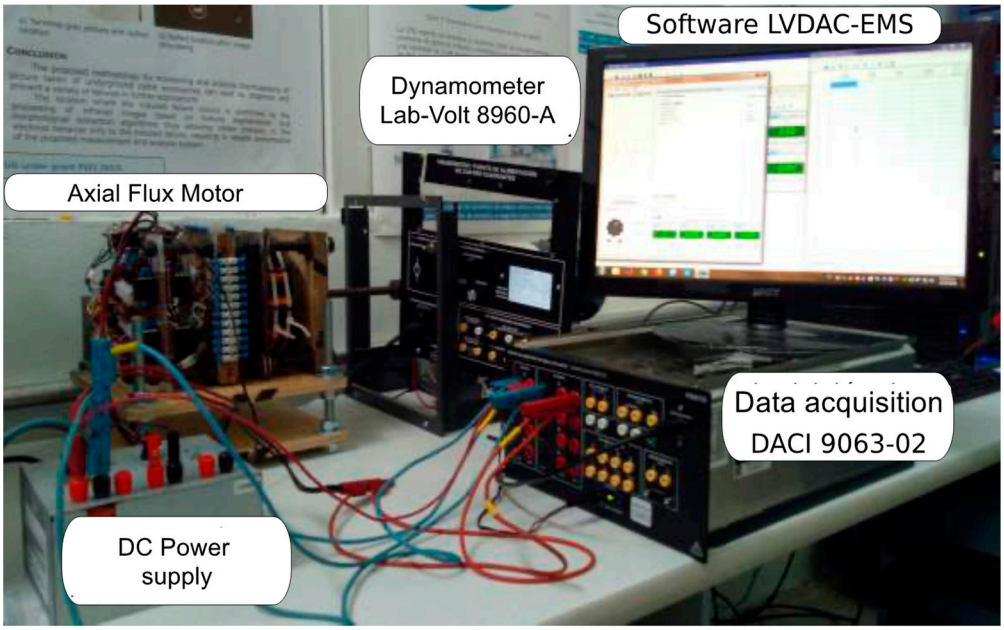

Figure 11. Measurement system used to measure and record the dynamic characteristics of the AFM.

3.3. Evaluation

The first dynamic characteristic measured was the change in angular velocity with respect to the change in the electrical supply frequency. The speed of the AFM was measured without load, while the electrical frequency was estimated by converting the digital switching frequency, developed by the speed control, into electrical frequency.

The comparison between the theoretical speed change and the actual measured speed, with respect to the change in electrical frequency, was made considering the calculation of the speed using Equation (20), with the same values of electrical frequency variation, applied with the system. evaluation for speed control.

Figure 12 shows the frequency graph with respect to angular velocity obtained from the simulation, with respect to the speed obtained from the evaluation of the motor, where on the horizontal axis, we have the electrical supply frequency, and on the vertical axis, the velocity produced in the AFM.

From these results, it is observed that there is a difference of 8.43% in the values obtained in the simulation with respect to the values measured in the AFM evaluation. Table 3 shows the maximum and minimum values of the evaluations with respect to the simulations.

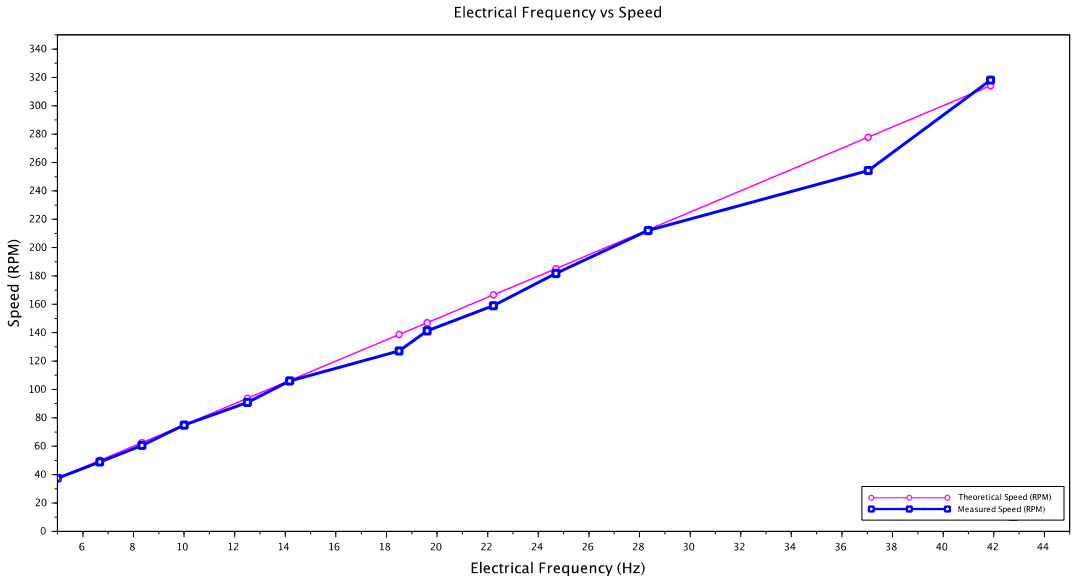

Figure 12. Plot of speed vs. electrical frequency of power supply in the AFM.

Table 3. Speed comparison between theoretical and measured.

	Speed (RPM)	
Characteristic	**Minimum**	**Maximum**
Theoretical	37.50	314.07
Measured	37.39	318.08
% Error	0.23	8.43

Table 4 shows the result of the maximum and minimum behavior for each of the control modes, with respect to the results obtained from the simulation and the evaluations carried out.

Table 4. Simulated and measured torque comparison (Nm).

Torque Conf.	**1**		**2**		**3**		**4**		**5**		**6**	
Parameters	**Min**	**Max**	**Min**	**Max**	**Min**	**Max**	**Min**	**Max**	**Min**	**Max**	**Min**	**Max**
Simulated	0.240	0.295	0.572	0.786	0.533	0.779	0.529	0.777	0.917	1.438	0.936	1.757
Measured	0.210	0.455	0.509	0.823	0.450	0.955	0.339	0.867	0.651	1.330	0.706	1.748
% Error	1.889	67.031	0.725	11.062	1.027	22.744	0.425	40.333	5.358	33.779	0.081	24.617

The presentation of a maximum error of 67%, with respect to the results obtained from the evaluations, is due to the low electromagnetic coupling with a reduced number of poles in the stator, according to configuration 1 [20].

Figure 13 shows a comparison of the torque with respect to the speed for each of the motor configurations, observing that for low speeds, there is a greater difference than for high speeds. These differences observed between the simulated values and those measured in configuration 1, or low speed, are due to the fact that there is a low electromagnetic coupling due to the synchronism speed between the rotor and the stator, observing an increase in the electric motor cogging.

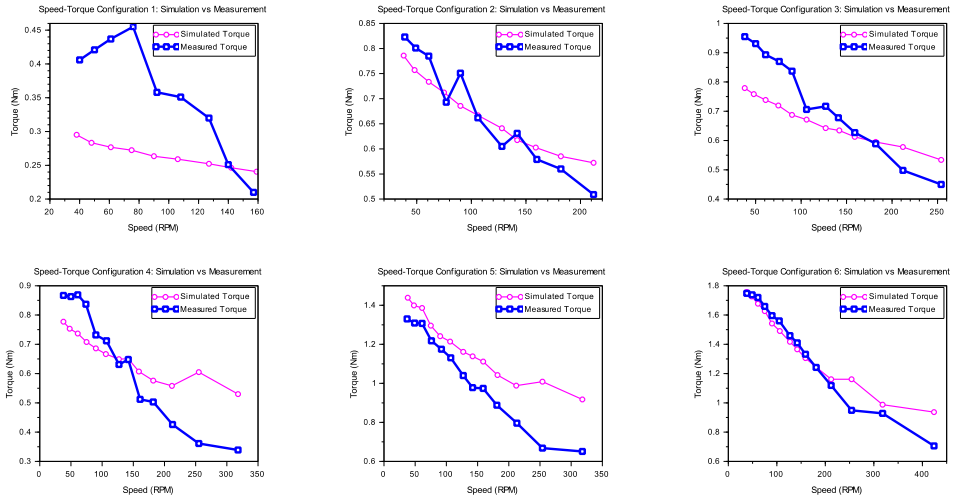

Figure 13. Plot of speed vs torque for the six AFM configurations (simulated and measured).

The evaluation of the power was carried out with respect to the speed delivered by the AFM, and as in the evaluation of the torque in relation to the speed, a low electromagnetic coupling is observed in configuration 1 compared to the rest of the configurations.

Plots of speed versus power are shown in Figure 14 for each of the six torque configurations.

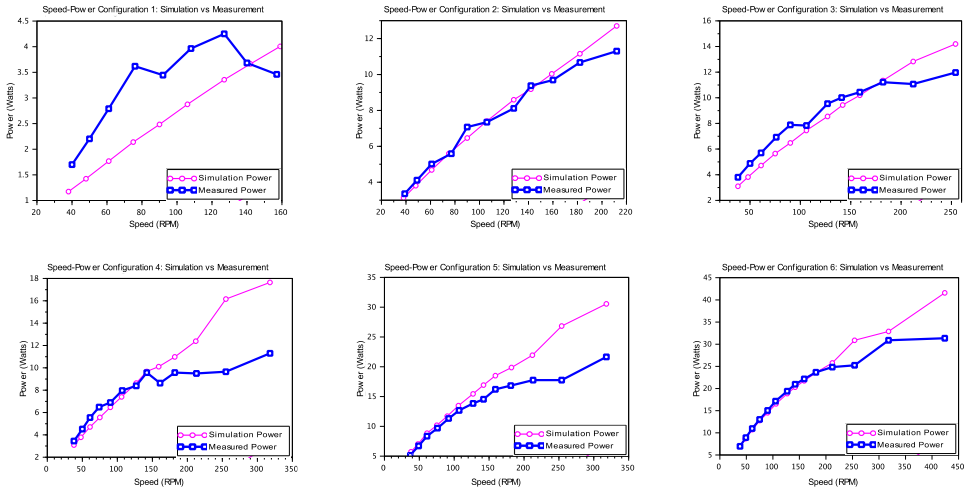

Figure 14. Plot of speed vs. power for the 6-torque configuration (simulated and measured).

In a similar way as in Figure 13, a decrease in Figure 14, the power supplied as a function of speed is observed, which represents a low electromagnetic coupling between the rotor and the stator.

The maximum and minimum results for each of the configurations are shown in Table 5, obtaining better performance for configuration 6.

Table 5. Simulated and measured power comparison (Watts).

Torque Conf.	**1**		**2**		**3**		**4**		**5**		**6**	
Parameters	**Min**	**Max**	**Min**	**Max**	**Min**	**Max**	**Min**	**Max**	**Min**	**Max**	**Min**	**Max**
Simulated	1.174	4.010	3.127	12.706	3.101	14.196	3.092	17.646	5.724	30.555	6.993	41.584
Measured	1.700	4.251	3.360	11.300	3.798	11.970	3.450	11.300	5.151	21.660	0.076	24.610
% Error	0.59	69.11	0.11	11.06	1.08	27.92	1.07	40.26	3.26	33.81	0.08	24.61

4. Conclusions

In this work, the bases for the design and construction of an electric machine in axial flow configuration, with U-type coils, were established, from commercial components for the design of the stator (magnetic cores) and the rotor (permanent magnets).

These consider that the operating conditions of the motor must be considered and based on this, the necessary power P_d must be specified for the specific application, considering the efficiency K_e and the work cycle K_d.

It was found that the best configuration for this application is the design of a motor considering a fourth order configuration, which represents 12 poles in the stator and 16 poles in the rotor, which interact with each other.

By means of a digital switching of stator poles, which changes its connection considering one coil per phase (configuration 1), until obtaining the maximum power with the connection of four coils per phase (configuration 6). The development of the control system has been previously published in [21], where the development and evaluation of the control system is shown in detail. The most outstanding advantages of the developed control are the absence of sensors for speed control, the omission of extra mechanisms to produce high torque at low speeds, its simple implementation, and the possibility of being extended to conventional configurations of radial flux motors.

For the optimization and verification of the design, the finite element modeling tool was used, with the particularity that this modeling was carried out by means of two separate simulations, considering the larger magnets of the external part of the rotor interacting with the stator coils and the modeling of the smaller magnets of the internal part, interacting with the same stator coils, finding differences between the simulated part and the real part of 8.43%, of speed regulation and with torques of 1.78 Nm, without having additional mechanical couplings.

Differences were found in the simulation of torque with respect to speed of up to 67% in the lower configurations, which is due to the lower electromagnetic coupling of the rotor with the stator at low speed, causing a greater cogging.

Author Contributions: Conceptualization, A.G.-P. and R.B.-T.; methodology, A.G.-P.; software, F.M.D.V.; validation, A.G.-P. and F.M.D.V.; formal analysis, and investigation, R.B.-T. and A.G.-P.; writing—original draft preparation, A.G.-P. and R.B.-T.; writing—review and editing, R.B.-T.; visualization, F.M.D.V.; project administration, A.G.-P.; funding acquisition, R.B.-T. All authors have read and agreed to the published version of the manuscript.

Funding: This research received no external funding.

Data Availability Statement: The original contributions presented in the study are included in the article, further inquiries can be directed to the corresponding author.

Conflicts of Interest: The authors declare no conflicts of interest.

References

1. Amin, S.; Khan, S.; Bukhari, S.S.H. A Comprehensive Review on Axial Flux Machines and Its Applications. In Proceedings of the 2019 2nd International Conference on Computing, Mathematics and Engineering Technologies (iCoMET), Sukkur, Pakistan, 30–31 January 2019; pp. 1–7. [CrossRef]
2. Xu, Z.; Li, T.; Zhang, F.; Zhang, Y.; Lee, D.H.; Ahn, J.W. A Review on Segmented Switched Reluctance Motors. *Energies* **2022**, *15*, 9212. [CrossRef]
3. Nasiri-Gheidari, Z.; Lesani, H. A Survey on Axial Flux Induction Motors. *Prz. Elektrotech.* **2012**, *88*, 300–305.
4. Gieras, F.; Wang, R.-J.; Kamper, M.J. *Axial Flux Permanent Magnet Brushless Machines*; Springer Science & Business Media: Berlin, Germany, 2004.
5. González-Parada, A.; Lozano-García, J.M.; Ibarra-Manzano, M.A. Digital Pole Control for Speed and Torque Variation in an Axial Flux Motor with Permanent Magnets. *Electronics* **2022**, *11*, 482. [CrossRef]
6. Krishnan, R.; Abouzeid, M.; Mang, X. A design procedure for axial field switched reluctance motors. In Proceedings of the Conference Record of the 1990 IEEE Industry Applications Society Annual Meeting, Seattle, WA, USA, 7–12 October 1990; Volume 1, pp. 241–246. [CrossRef]

7. Materu, P.; Krishnan, R. Analytical prediction of SRM inductance profile and steady-state average torque. In Proceedings of the Conference Record of the 1990 IEEE Industry Applications Society Annual Meeting, Seattle, WA, USA, 7–12 October 1990; Volume 1, pp. 214–223. [CrossRef]
8. Aydin, M.; Huang, S.; Lipo, T.A. Axial flux permanent magnet disc machines: A review. *Conf. Record SPEEDAM* **2004**, *8*, 61–71.
9. Lambert, T.; Biglarbegian, M.; Mahmud, S. A Novel Approach to the Design of Axial-Flux Switched-Reluctance Motors. *Machines* **2015**, *3*, 27–54. [CrossRef]
10. Shao, L.; Navaratne, R.; Popescu, M.; Liu, G. Design and construction of axial-flux permanent magnet motors for electric propulsion applications—A review. *IEEE Access* **2021**, *9*, 158998–159017. [CrossRef]
11. Abdullah, H.; Ramasamy, G.; Ramar, K.; Aravind, C.V. Design consideration of dual axial flux motor for electric vehicle applications. In Proceedings of the IEEE Conference on Energy Conversion (CENCON), Johor Bahru, Malaysia, 19–20 October 2015; pp. 72–77.
12. Caricchi, F.; Crescimbini, F.; Honrati, O. Modular axial-flux permanent-magnet motor for ship propulsion drives. *IEEE Trans. Energy Convers.* **1999**, *14*, 673–679. [CrossRef]
13. Dianati, B.; Kahourzade, S.; Mahmoudi, A. Optimization of axial-flux induction motors for the application of electric vehicles considering driving cycles. *IEEE Trans. Energy Convers.* **2020**, *35*, 1522–1533. [CrossRef]
14. Nielsen, S.S.; Jæger, R.; Rasmussen, P.O.; Kongerslev, K. Development and analysis of double U-core switched reluctance machine. In Proceedings of the IEEE International Electric Machines and Drives Conference (IEMDC), Miami, FL, USA, 21–24 May 2017. [CrossRef]
15. Ostovic, V. Performance comparison of U-Core and round-stator single-phase permanent-magnet motors for pump applications. *IEEE Trans. Ind. Appl.* **2002**, *38*, 476–482. [CrossRef]
16. Deng, X.; Mecrow, B.; Wu, H.; Martin, R. Design and development of low torque ripple variable-speed drive system with six-phase switched reluctance motors. *IEEE Trans. Energy Convers.* **2017**, *33*, 420–429. [CrossRef]
17. Andrada Gascón, P. Design of a segmented switched reluctance drive for a light electric vehicle. *Renew. Energy Power Qual. J.* **2022**, *20*, 662–667. [CrossRef]
18. Marcsa, D.; Kuczmann, M. Design and control for torque ripple reduction of a 3-phase switched reluctance motor. *Comput. Math. Appl.* **2017**, *74*, 89–95. [CrossRef]
19. Kalaivani, L.; Subburaj, P.; Iruthayarajan, M.W. Speed control of switched reluctance motor with torque ripple reduction using non-dominated sorting genetic algorithm (NSGA-II). *Int. J. Electr. Power Energy Syst.* **2013**, *53*, 69–77. [CrossRef]
20. Al-Amyal, F.; Hamouda, M.; Szamel, L. Performance improvement based on adaptive commutation strategy for switched reluctance motors using direct torque control. *Alex. Eng. J.* **2022**, *61*, 9219–9233. [CrossRef]
21. Jæger, R.; Nielsen, S.S.; Rasmussen, P.O. Theoretical evaluation of the double U-core switched reluctance machine. In Proceedings of the 2017 IEEE International Electric Machines and Drives Conference (IEMDC), Miami, FL, USA, 21–24 May 2017. [CrossRef]